Preprints.org

Hypothesis

Not peer-reviewed version

Two Substrates, One Switch: Oxygen and Iodine as the Mechanistic Basis of the Three-Armed HIF-1α Severity Cascade in SARS-CoV-2 Infection

Stuart G. Ashbaugh *

Posted Date: 7 April 2026

doi: 10.20944/preprints202604.0439.v1

Keywords: HIF-1α; DUOX; lactoperoxidase; iodine; hypoiodous acid; DLI axis; Furin; SARS-CoV-2; silent hypoxia; mechanistic hypothesis

Preprints.org is a free multidisciplinary platform providing preprint service that is dedicated to making early versions of research outputs permanently available and citable. Preprints posted at Preprints.org appear in Web of Science, Crossref, Google Scholar, Scilit, Europe PMC.

Copyright: This open access article is published under a Creative Commons CC BY 4.0 license, which permit the free download, distribution, and reuse, provided that the author and preprint are cited in any reuse.

Preprints.org (www.preprints.org) | NOT PEER-REVIEWED | Posted: 7 April 2026 doi:10.20944/preprints202604.0439.v1

Disclaimer/Publisher's Note: The statements, opinions, and data contained in all publications are solely those of the individual author(s) and contributor(s) and not of MDPI and/or the editor(s). MDPI and/or the editor(s) disclaim responsibility for any injury to people or property resulting from any ideas, methods, instructions, or products referred to in the content.

Hypothesis

Two Substrates, One Switch: Oxygen and Iodine as the Mechanistic Basis of the Three-Armed HIF-1α Severity Cascade in SARS-CoV-2 Infection

Stuart G. Ashbaugh

Sigma Xi, The Scientific Research Honor Society, Sequim, Washington 98382, USA; sgashbaugh@gmail.com

Abstract

Severe COVID-19 follows a cliff-edge trajectory: patients appear stable, then deteriorate rapidly and irreversibly. This paper identifies molecular oxygen as the dual control variable governing two previously unconnected biological systems: the DUOX-Lactoperoxidase-Iodine (DLI) airway antiviral defense and HIF-1α, the transcription factor that drives COVID-19 severity. Both share the same oxygen-dependent enzymes (DUOX and PHD, Km approximately 20 μM O_2 corresponding to approximately 94% SpO_2). When SpO_2 falls below this threshold via AT2 cell destruction with surfactant loss, ventilation-perfusion mismatch, and microvascular thrombosis, both systems fail simultaneously, initiating three concurrent cascade arms: (1) collapse of DLI mucosal defense through O_2 substrate depletion; (2) HIF-1α-driven Furin upregulation accelerating viral spike cleavage and entry, with a viral amplification feedback loop; and (3) IL-6-mediated cytokine storm depleting thyroid iodide reserves. These three arms interact multiplicatively, not additively. A Monte Carlo simulation across four populations demonstrates a 40.3% steeper cliff-edge signature than an additive null model. The framework generates three falsifiable clinical predictions and identifies supplemental oxygen initiated before the HIF-1α threshold (SpO_2 94–95%) as the primary actionable intervention, suppressing all three cascade arms simultaneously.

Keywords: HIF-1α; DUOX; lactoperoxidase; iodine; hypoiodous acid; DLI axis; Furin; SARS-CoV-2; silent hypoxia; mechanistic hypothesis

---

1. The DLI Axis: Established Mechanistic Evidence

1.1. DUOX Enzymes and H_2O_2 Generation

The Dual Oxidase (DUOX) family — comprising DUOX1 and DUOX2 — are transmembrane enzymes anchored on the apical plasma membrane of ciliated respiratory epithelial cells. They produce hydrogen peroxide (H_2O_2) via electron transfer from intracellular nicotinamide adenine dinucleotide phosphate (NADPH) to molecular oxygen in the airway surface liquid: $NADPH + 2O_2 \rightarrow NADP^+ + H^+ + 2H_2O_2$ [52]. DUOX1 localizes to ciliated airway cells and is the primary source of extracellular H_2O_2 under basal conditions [26]. DUOX2 is more strongly induced during viral infection; it is among the top ten most upregulated metabolic genes in SARS-CoV-2-infected airway epithelial cells [13]. Both enzymes require molecular oxygen as an obligate electron acceptor — without adequate O_2, H_2O_2 production ceases. This is a biochemical absolute, not a regulatory preference. This oxygen dependency has direct in vivo relevance to COVID-19: molecular characterisation of excised COVID-19 lung tissue identified molecular features of chronic epithelial hypoxia — including increased EGLN3 expression, a specific marker for hypoxic airway epithelial cells — in airways lining mucus-obstructed regions, confirming that SARS-CoV-2 infection creates the localised airway hypoxia that the DLI substrate-depletion mechanism requires [43].

The antiviral role of DUOX-derived reactive oxygen species (ROS) has been established beyond cell culture [19]. In vivo silencing of DUOX increased viral load during H1N1 influenza infection in

© 2026 by the author(s). Distributed under a Creative Commons CC BY license.

Preprints.org (www.preprints.org) | NOT PEER-REVIEWED | Posted: 7 April 2026 doi:10.20944/preprints202604.0439.v1

an animal model, providing the first in vivo evidence linking DUOX NADPH oxidases directly to mammalian antiviral defense [19]. DUOX2 promoter single-nucleotide polymorphisms (SNPs) further explain inter-individual variability in antiviral defense capacity, providing a molecular basis for outcome heterogeneity that comorbidity and age models cannot capture [10].

The H_2O_2 that DUOX produces does not act as an antiviral agent on its own. It is the substrate for lactoperoxidase (LPO), which uses it to generate hypoiodous acid (HOI) — the actual virucidal agent.

1.2. Lactoperoxidase and Hypoiodous Acid

Lactoperoxidase (LPO), secreted by submucosal glands into the airway surface liquid, catalyzes the two-electron oxidation of iodide in the presence of DUOX-derived H_2O_2: $I^- + H_2O_2 \rightarrow HOI + OH^-$. Hypoiodous acid (HOI) inactivates respiratory viruses by oxidizing histidine and tyrosine residues conserved across SARS-CoV-2 variants in the spike protein receptor-binding domain, preventing engagement with angiotensin-converting enzyme 2 (ACE2), the host cell surface receptor SARS-CoV-2 uses for entry [7,11]. This mechanism achieves 99% viral inactivation within 30–60 seconds and is variant-independent [27]. In vivo confirmation that airway iodide concentration directly governs respiratory virus severity comes from an ovine model of respiratory syncytial virus (RSV) infection: oral potassium iodide supplementation produced a 10-fold increase in airway surface liquid iodide concentration and significantly reduced lung lesion scores, RSV antigen expression, and IL-8 levels compared to unsupplemented controls; inhibition of LPO activity reversed this protection [44]. This is the closest existing in vivo evidence that the iodide-LPO-HOI axis determines antiviral defense competence in a respiratory virus analogous to SARS-CoV-2.

Clinical corroboration of the iodine/LPO mechanism comes from multiple international trials. A Phase II randomized double-blinded placebo-controlled trial of 0.5% povidone-iodine nasal spray conducted in South Africa (2022–2023) eliminated SARS-CoV-2 viral nasal shedding after 4–5 days of multi-dose treatment [8]. An Egyptian randomized trial found that combined nasal and oropharyngeal iodine delivery accelerated clinical and laboratory recovery and reduced household transmission [6]. A Saudi Arabian RCT demonstrated statistically significant reduction in viral survival days with 0.23% povidone-iodine nasal rinses [1]. A Japanese randomized trial demonstrated gargling with povidone-iodine produced short-term inhibitory effects on SARS-CoV-2 [16]. This cross-continental trial evidence from Africa, the Middle East, Japan, and Egypt transforms the iodine/HOI virucidal mechanism from primarily in vitro to clinically corroborated. Critically, however, not all povidone-iodine trials were positive: a triple-blinded randomized controlled trial (RCT) found no statistically significant reduction in nasopharyngeal viral load with 0.5% or 2.0% povidone-iodine (PVP-I) nasal spray versus saline in outpatients [34]. Results have varied with concentration, route, and timing [33], confirming that iodine delivery is the operative variable, not iodine sufficiency per se [2,8].

Understanding which populations are most vulnerable to DLI axis failure requires establishing how widely iodine — the substrate the system depends on — is deficient globally.

1.3. Iodine Deficiency: Global Burden

Global iodine deficiency incidence was 8.08 million cases in 2021 and is projected to reach 8.48 million by 2050 [14]. The Iodine Global Network (2025) reports 21 countries still with insufficient iodine status, down from 113 in 1993 [12]. In the WHO European Region, mild deficiency remains widespread in vulnerable subgroups despite reduction from 23 deficient countries in 2003 to 2 in 2023 [29]. The at-risk populations for iodine deficiency include parts of inland sub-Saharan Africa, South and Central Asia, and mountainous regions globally.

Japanese dietary iodine intake is considerably higher than the commonly cited “2× US RDA” figure. Estimates based on dietary records, food surveys, and urine iodine analysis place average Japanese intake from seaweed at 1,000–3,000 μg/day — approximately 7–20× the US recommended dietary allowance (RDA) of 150 μg/day [32]. A follow-up analysis confirmed that Japan’s COVID-19

© 2026 by the author(s). Distributed under a Creative Commons CC BY license.

Preprints.org (www.preprints.org) | NOT PEER-REVIEWED | Posted: 7 April 2026 doi:10.20944/preprints202604.0439.v1

mortality advantage relative to other developed nations persisted through March 2023 [25]. However, younger Japanese adults consuming Westernized diets have substantially lower iodine intakes, and the protective signal may therefore reflect older-generation dietary patterns rather than population-wide intake.

The DLI axis — however well-supplied with iodide — is rendered inoperable when its upstream oxygen substrate is withdrawn. The mechanism by which that withdrawal triggers system-wide collapse is governed by a single transcription factor.

1.4. HIF-1α Biology and Activation Threshold

Under normal oxygen levels, HIF-1α is continuously made but rapidly degraded. PHD enzymes require molecular oxygen as an obligate co-substrate to hydroxylate HIF-1α at Pro402 and Pro564, marking it for degradation. The Michaelis constant (K_M) for oxygen in PHD reactions is approximately 20 μM — equivalent to the oxygen tension at arterial SpO_2 of approximately 94% [52]. This K_M value is the mechanistic basis of the 94% threshold: as SpO_2 falls below this point, PHD enzymes enter the substrate-limiting range and HIF-1α begins to accumulate. Critically, DUOX enzymes share this same oxygen dependency, with a functionally equivalent threshold — the molecular basis of the inverse HIF-1α/DUOX relationship described in Section 2. Below approximately 94% SpO_2, PHD activity declines, HIF-1α escapes degradation, accumulates, and translocates to the nucleus to activate hundreds of target genes via hypoxia-response elements (HREs) [4]. The 2025 HIF-1α scoping review [22] confirmed that serum HIF-1α above 4.8 ng/mL is an independent predictor of silent hypoxia severity with an area under the receiver operating characteristic curve (AUC) of 0.89, validating HIF-1α as a measurable cascade biomarker.

HIF-1α drives anaerobic glycolysis (upregulating lactate dehydrogenase A (LDHA) and 6-phosphofructo-2-kinase/fructose-2,6-bisphosphatase 3 (PFKFB3)) and increases vascular endothelial growth factor (VEGF)-driven angiogenesis — both established downstream effects independent of COVID-19 [15]. It also co-activates Nuclear Factor kappa B (NF-κB) — a transcription factor that drives inflammatory gene expression — to amplify cytokine production, and upregulates Furin (a host endoprotease that cleaves the SARS-CoV-2 spike protein at the S1/S2 junction, substantially enhancing infectivity) via HREs in its promoter [22]. The specific claim that HIF-1α upregulates Furin consistently across tissue types is supported; the claim that it upregulates ACE2 in airway epithelium is not — pulmonary tissue data show HIF-1α generally suppresses ACE2 [22,31]. Arm 2 of the proposed cascade is therefore correctly based on Furin, not ACE2 upregulation in the lung.

HIF-1α also initiates a third attack on the DLI axis. This one operates through the inflammatory cascade and targets the iodide supply directly.

1.5. Thyroid Dysfunction and IL-6-Driven Iodide Sequestration

Non-thyroidal illness syndrome (NTIS) — the suppression of type 1 and type 2 iodothyronine deiodinase enzyme activity (D1 and D2) by inflammatory cytokines, reducing thyroxine (T4) to triiodothyronine (T3) conversion — is well-established in severe illness of any cause [21]. In COVID-19, elevated interleukin-6 (IL-6) — a major pro-inflammatory cytokine — suppresses D1 enzyme activity, diminishing T3 synthesis and reducing circulating iodide availability [5,21]. Tumor necrosis factor alpha (TNF-α)-mediated NF-κB activation further disrupts D1 promoter activity [5]. The cytokine storm's impact on thyroid function is among the most replicated non-pulmonary findings in COVID-19 endocrinology, confirmed across Italian, Greek, and Danish cohorts and in multiple systematic reviews through 2024 [5,21]. The author identifies the implication of this mechanism for LPO iodide substrate availability as a novel connection proposed in this paper.

This thyroid-mediated iodide sequestration occurs precisely because the patient is hypoxic. In COVID-19, that hypoxia is frequently invisible until the cascade threshold has already been crossed.

The downstream consequence of this iodide sequestration mechanism has been measured, if not directly attributed to iodide depletion, in multiple COVID-19 clinical studies. Non-thyroidal illness syndrome (NTIS) — characterised by low free T3 (fT3) with normal or low TSH and T4 — is the most

© 2026 by the author(s). Distributed under a Creative Commons CC BY license.

Preprints.org (www.preprints.org) | NOT PEER-REVIEWED | Posted: 7 April 2026 doi:10.20944/preprints202604.0439.v1

common thyroid abnormality in hospitalised COVID-19 patients, with a prevalence of 27–64% depending on disease severity [49,51]. Critically, fT3 levels at admission are an independent predictor of mortality, mechanical ventilation, and ICU transfer in COVID-19 patients [49,51]. A 276-patient retrospective study found the fT3/rT3 ratio was significantly lower in ICU patients than in ward patients (3.96 vs 5.00 pg/ng, $p = 0.007$), confirming impaired peripheral thyroid hormone conversion proportional to disease severity [50]. IL-6 is established as the primary driver of this NTIS pattern: an inverse correlation between serum T3 and IL-6 in hospitalised patients has been observed since the 1990s and has been replicated in COVID-19 cohorts [51]. This body of evidence confirms that the cytokine-driven deiodinase suppression described in this arm of the cascade is occurring in COVID-19 patients at a clinically significant scale. What has not been measured is the downstream consequence for airway iodide availability and HOI production — the mechanistic link that Trial 1 in Section 3.7.4 is designed to establish.

1.6. Silent Hypoxia and SpO_2 Trajectories

Silent hypoxia — in which tissue oxygen is critically low while patients feel no dyspnea — arises from three independently established mechanisms that together reduce arterial oxygen saturation without triggering the dyspnea response. First, SARS-CoV-2 preferentially infects and destroys alveolar type II (AT2) pneumocytes, which are the primary producers of pulmonary surfactant. Surfactant prevents alveolar collapse by reducing surface tension at the air–liquid interface; as AT2 cells are lost, surfactant production falls, alveoli collapse or fill with protein-rich fluid, and the effective surface area for gas exchange shrinks [45]. Second, this alveolar damage produces severe ventilation–perfusion (V/Q) mismatch: blood continues to flow through alveoli that can no longer oxygenate it. Critically, the normal homeostatic reflex — hypoxic pulmonary vasoconstriction, which redirects blood away from poorly ventilated alveoli — is lost in COVID-19 ARDS, allowing deoxygenated blood to enter the arterial circulation [46]. Third, inflammation and endothelial injury promote microvascular thrombosis and pulmonary vascular occlusion, creating perfusion dead space and further impairing gas exchange [48]. The claim that viral proteins directly attack haemoglobin and strip iron from the heme group has not been supported by clinical evidence: no significant haemolysis has been documented in COVID-19 cohorts, and erythrocytes lack the cellular machinery to produce viral proteins [47]. Arterial oxygen saturation therefore falls because gas exchange is mechanically impaired, not because the oxygen carrier is damaged. SpO_2 ≤88% is an independent predictor of mortality in COVID-19 [3]. In a Kenyan cohort of 1,124 hospitalized COVID-19 patients, 81.4% had hypoxia at admission and 39.9% had no respiratory distress, confirming silent hypoxia in a sub-Saharan African population and validating its clinical relevance internationally [28].

Silent hypoxia does not only impair oxygen delivery — it leaves a metabolic signature readable at the bedside. That signature is blood pH.

1.7. Blood pH: A Downstream Marker of Cascade Initiation

Blood pH acidosis in severe COVID-19 is a consequence of HIF-1α-driven anaerobic glycolysis: upregulation of LDHA and PFKFB3 accelerates lactate production, depleting serum bicarbonate and lowering arterial pH below the normal range of 7.35–7.45. The author identifies this as a downstream metabolic consequence of cascade initiation, not an independent causal variable. Siebert et al. [23] demonstrated significantly lower blood pH in fatal versus surviving COVID-19 ICU patients across a 25-patient cohort, providing direct clinical evidence that lower pH tracks cascade progression. When blood pH is low, three things are already true: HIF-1α has been active, DUOX has lost O_2 substrate, and iodide depletion via IL-6-driven deiodinase suppression is underway. The author therefore characterizes blood pH as a composite severity marker — a readable downstream indicator of cascade stage accessible at any bedside without specialised assays.

The author draws an important clinical implication from this: correcting blood pH without addressing the underlying HIF-1α cascade — for instance, with bicarbonate administration — would not be expected to substantially alter the disease trajectory. The low pH is the readout, not the driver.

© 2026 by the author(s). Distributed under a Creative Commons CC BY license.

Preprints.org (www.preprints.org) | NOT PEER-REVIEWED | Posted: 7 April 2026 doi:10.20944/preprints202604.0439.v1

This distinction has direct bearing on clinical decision-making: a falling pH should prompt immediate attention to SpO_2 maintenance and cascade stage assessment, not pH correction in isolation. Blood pH is best understood as one of the four inputs to the proposed DLI Competency Index (Section 7.3), where it contributes a metabolic cascade progression signal alongside SpO_2, urinary iodide, and serum HIF-1α.

Blood pH reflects cascade progression at the systemic level. A separate pH mechanism operates independently at the subcellular level — governing not cascade severity but the speed of viral trafficking into the cell itself.

1.8. NHE9 and Endosomal pH

Early endosomal pH (6.0–6.5) governs SARS-CoV-2 trafficking from early to late endosomes, where cathepsin L (a lysosomal cysteine protease)-mediated spike cleavage enables membrane fusion. NHE9 (sodium-proton exchanger 9), encoded by SLC9A9, raises endosomal pH by pumping protons out. A Swedish/German study [20] demonstrated that NHE9 overexpression raises early endosomal pH by 0.84 units, inhibits phosphatidylinositol-3-phosphate (PI3P) depletion from endosomal membranes, and impairs SARS-CoV-2 spike delivery to late endosomes — slowing viral entry. NHE9 is the only endosomal pH regulator genetically linked to COVID-19 severity risk [20]. This mechanism integrates directly with the cascade framework as a parallel implementation of Arm 2: where Furin mediates extracellular spike cleavage at the cell surface (Section 3.2), cathepsin L mediates intracellular spike cleavage in the endosome — and both are enhanced when NHE9 expression is high and HIF-1α is active. Maintaining SpO_2 above 94% suppresses HIF-1α, which reduces both Furin and NHE9-mediated entry enhancement simultaneously. This makes early oxygen intervention doubly protective against viral entry via Arm 2 mechanisms. Together, these independently established mechanisms form the biological foundation from which the synthesis in Section 2 is constructed.

2. The Novel Synthesis: Oxygen as the Dual Control Variable

Each component described in Section 1 is independently established. The author identifies a single mechanistic link that connects them into a self-amplifying cascade: molecular oxygen is the common substrate and cofactor of both the DLI defense (via DUOX, Section 1.1) and the cascade suppressor (via PHD enzymes, Section 1.4). Below approximately 94% SpO_2, both functions fail simultaneously — from the same threshold, at the same moment, as a direct consequence of the same physiological event. To the author's knowledge, this dual role of molecular oxygen — as the simultaneous biochemical substrate for the DLI defense and the enzymatic cofactor that suppresses the HIF-1α severity cascade — has not been previously described in integrated form in the COVID-19 literature or in respiratory immunology more broadly. It is this connection, and not any individual component, that constitutes the primary scientific contribution of this work.

Critically, because the cascade is triggered by host physiology — SpO_2 falling below the shared PHD/DUOX oxygen threshold — rather than by any variant-specific viral protein, the framework applies irrespective of the infecting variant. Alpha, Delta, Omicron, and any future SARS-CoV-2 lineage all infect human airway epithelium and can drive hypoxia in severe cases; none repeal the biochemistry of PHD enzyme oxygen dependency or DUOX substrate requirements.

The cascade architecture that follows from this dual-substrate insight is not a collection of three independent observations about COVID-19 severity. It is the mechanistic consequence of a single quantitative fact: both systems fail at the same oxygen tension because they share the same enzymatic oxygen requirement. This is why the deterioration is simultaneous rather than sequential, and why it is abrupt rather than gradual. A patient who crosses 94% SpO_2 does not experience the collapse of one defense, then adapt, then experience another. All three consequences begin at the same moment from the same molecular cause.

This also explains why the cascade has proved difficult to interrupt clinically. Interventions targeting a single arm (anti-cytokine therapy for Arm 3, antiviral entry inhibitors for Arm 2) address

© 2026 by the author(s). Distributed under a Creative Commons CC BY license.

Preprints.org (www.preprints.org) | NOT PEER-REVIEWED | Posted: 7 April 2026 doi:10.20944/preprints202604.0439.v1

one downstream consequence without affecting the oxygen threshold that triggered all three. The framework predicts that only oxygen itself — maintaining SpO_2 above the shared PHD/DUOX threshold before it is crossed — can suppress all three arms simultaneously. Every subsequent section of this paper elaborates consequences of this single mechanistic observation.

3. The Three-Armed Cascade

3.1. Arm 1: HIF-1α Dismantles the DLI Defense

When SpO_2 falls below ~94%, PHD activity declines and HIF-1α stabilizes [4,22]. Concurrently, DUOX loses the O_2 electron acceptor required for H_2O_2 generation [26,52] — both events are immediate consequences of the same threshold breach. HIF-1α then activates anaerobic glycolysis (LDHA, PFKFB3) [15], which accelerates further SpO_2 decline, compounding DUOX substrate depletion in a self-reinforcing spiral: lower SpO_2 drives more HIF-1α stabilization, which drives more anaerobic glycolysis, which produces more lactate and further impairs respiratory function — each turn of the loop tightening the next. From the biochemistry in Sections 1.1 and 1.2, the author infers that HOI production does not decline linearly. It collapses non-linearly as the positive feedback loop tightens.

3.2. Arm 2: HIF-1α Upregulates Furin, Accelerating Viral Entry

Furin is an enzyme that cleaves precursor proteins at multi-basic amino acid recognition sequences; it is the host protease responsible for cleaving the SARS-CoV-2 spike protein at the S1/S2 junction, a step that substantially enhances viral infectivity and cell-to-cell spread. Furin promoters contain functional HREs consistently activated by HIF-1 heterodimers across tissue types [4], meaning HIF-1α stabilization directly upregulates the very enzyme that makes viral entry more efficient. Furin-mediated cleavage of the spike S1/S2 junction substantially enhances infectivity [41], and HIF-1α activation therefore progressively prepares the cellular proteolytic landscape for more efficient viral entry with each replication cycle.

Because SARS-CoV-2 binds host cells via the ACE2 receptor, one might expect HIF-1α-driven upregulation of ACE2 to be the dominant viral entry mechanism under hypoxia. However, the evidence does not support this in the primary target tissue: in pulmonary epithelium, HIF-1α generally suppresses rather than upregulates ACE2 [22,31]. The net viral entry acceleration in the airway therefore operates via Furin efficiency, not ACE2 receptor density.

This distinction has a critical mechanistic consequence that is unique to Arm 2: the viral amplification loop closes back onto the oxygen variable. Enhanced Furin-mediated entry means more viral replication within AT2 cells, which are the primary target for SARS-CoV-2 in the lower respiratory tract. More AT2 cell destruction means further loss of surfactant, deeper V/Q mismatch, and steeper SpO_2 decline — which in turn drives PHD enzyme suppression, more HIF-1α accumulation, and still more Furin upregulation. Arm 2 is therefore not merely an amplifier of viral entry — it is the mechanism by which the virus actively worsens the hypoxia that initiated all three cascade arms.

3.3. Arm 3: HIF-1α Drives Cytokine Storm and Iodide Depletion

HIF-1α co-activates with NF-κB, driving IL-6, TNF-α, and interleukin-1 beta (IL-1β) production [15]. The resulting cytokine storm then suppresses D1 and D2 deiodinase enzymes via IL-6 [5,21], as established in Section 1.5, sequestering the thyroid iodide reservoir at precisely the moment when LPO substrate is most critically needed. Together, the three arms encircle and dismantle the DLI axis: Arm 1 removes oxygen, Arm 2 accelerates Furin-mediated viral entry, and Arm 3 removes iodide — a mechanism that becomes catastrophic only because the HOI that would have oxidized and inactivated the spike protein before cell contact has already been depleted by Arms 1 and 3.

© 2026 by the author(s). Distributed under a Creative Commons CC BY license.

Preprints.org (www.preprints.org) | NOT PEER-REVIEWED | Posted: 7 April 2026 doi:10.20944/preprints202604.0439.v1

Table 1. Three-arm cascade summary matrix. Each arm is triggered simultaneously at the ~94% SpO_2 threshold by a common cause (HIF-1α stabilisation), but operates via a distinct substrate and mechanism and becomes fully active at different lags post-threshold. Arms 1 and 3 act as brakes removed; Arm 2 acts as an accelerant added. Their interaction is multiplicative: Reduced defense (Arm 1) × Accelerated viral entry (Arm 2) × Iodide depletion (Arm 3) = exponential cliff-edge deterioration.

Arm	Trigger	Substrate / Target	Mechanism	Stages Active	Interaction Role
Arm 1 DLI Defense Collapse	SpO_2 < ~94% (PHD fails; DUOX loses O_2)	O_2 (DUOX electron acceptor)	DUOX loses H_2O_2 output → LPO loses substrate → HOI production ceases. Spike protein no longer inactivated.	Steps 3–10 (immediate at threshold)	*BRAKE REMOVED Reduces defense (multiplicative denominator)*
Arm 2 Furin Upregulation	HIF-1α binds HREs in Furin promoter	Spike S1/S2 cleavage efficiency	Furin expression rises; more efficient spike cleavage → faster viral entry → more AT2 destruction → deeper SpO_2 decline (feedback loop).	Steps 4–10 (lag ~hours post-threshold)	*ACCELERANT ADDED Increases viral entry efficiency (multiplicative numerator)*
Arm 3 Iodide Depletion	HIF-1α → NF-κB → IL-6 surge suppresses D1/D2 deiodinases	Thyroid iodide reserve (LPO substrate)	IL-6 suppresses D1/D2 → T4→T3 conversion blocked → iodide sequestered in thyroid → LPO loses I^- substrate → HOI ceases even if DUOX recovered.	Steps 5–10 (2–4 day lag post-threshold)	*BRAKE REMOVED Depletes iodide substrate (compounds Arm 1 multiplicatively)*

3.4. Why Exponential, Not Linear, Kinetics

The three arms are simultaneous, not sequential. Arms 1 and 3 each remove a brake on viral replication — collapsing the HOI mucosal barrier and sequestering the iodide substrate the LPO system requires, respectively. Arm 2 adds the accelerant: Furin upregulation increases viral entry efficiency, a gain that is inconsequential when HOI is present at protective concentrations but

© 2026 by the author(s). Distributed under a Creative Commons CC BY license.

Preprints.org (www.preprints.org) | NOT PEER-REVIEWED | Posted: 7 April 2026 doi:10.20944/preprints202604.0439.v1

devastating once Arms 1 and 3 have sufficiently depleted it below the threshold required for effective viral inactivation.

The author proposes that their combined effect is multiplicative: reduced defense (Arm 1) × expanded entry efficiency (Arm 2) × unchecked inflammation completing iodide depletion (Arm 3) — a logical inference from the simultaneous activation of three independently adverse processes rather than a directly measured kinetic parameter. This multiplicative architecture is proposed to produce the approximately exponential deterioration kinetics — the cliff-edge — that sequential, additive models cannot explain.

The multiplicative cascade architecture has a precise mathematical expression. Treating each arm as a coupled differential equation, viral clearance rate is governed by the inequality $r \cdot F(H) > k_{vir} \cdot O$, where r is the viral replication rate, $F(H) = 1 + (F_{max} - 1) \cdot H$ is the HIF-1α-driven Furin upregulation function, k_{vir} is the HOI virucidal rate constant, and O is HOI concentration. When this inequality holds, viral load grows faster than HOI can clear it — the system has crossed into the severe attractor's basin. The full six-variable ODE system, phase portrait, and bifurcation analysis are provided in Appendix A.

3.5. The Ten-Step Cascade Summary

Table 2 summarizes the ten-step HIF-1α-driven cascade. Steps 1–2 reflect the pre-threshold window. Step 3 is the threshold event. Steps 3–5 are the most clinically dangerous window — cascade initiated but patient may appear stable. Steps 6–10 reflect irreversible progression.

Table 2. The ten-step HIF-1α-driven cascade. Steps 1–2 reflect the pre-threshold window. Step 3 is the threshold event. Steps 3–5 are the most clinically dangerous window — cascade initiated but patient may appear stable. Steps 6–10 reflect irreversible progression.

Step	Phase	Arms Active	Event / Cascade State
1	Pre-threshold	*None (DLI intact)*	Viral entry; initial replication; DLI axis functional; patient asymptomatic or mildly symptomatic.
2	Pre-threshold	*None (DLI intact)*	SpO_2 begins falling via AT2 cell destruction (surfactant loss), V/Q mismatch, and microvascular thrombosis. Silent hypoxia. HIF-1α still suppressed by PHD enzymes above threshold.
3	THRESHOLD EVENT	*Arms 1+2+3 initiated*	SpO_2 crosses ~94%; PHD activity falls; HIF-1α accumulates; DUOX O_2 substrate depleted. All three cascade arms activate simultaneously.
4	Early cascade	*Arm 1 + Arm 2*	HIF-1α activates anaerobic glycolysis and upregulates Furin; Furin-mediated viral entry accelerates AT2 destruction, steepening SpO_2 decline. Viral amplification feedback loop begins. HOI falls below protective concentration.
5	Early cascade	*Arm 3 initiating*	NF-κB co-activation; IL-6 surge begins; thyroid iodide sequestration starts. Patient may still appear stable.
6	Mid cascade	*All 3 arms*	Anaerobic glycolysis lowers blood pH; SpO_2 worsens; self-reinforcing spiral accelerates.
7	Mid cascade	*All 3 arms*	Viral load surges via efficient Furin-mediated entry; HOI barrier gone; iodide reserves exhausted.

© 2026 by the author(s). Distributed under a Creative Commons CC BY license.

Preprints.org (www.preprints.org) | NOT PEER-REVIEWED | Posted: 7 April 2026 doi:10.20944/preprints202604.0439.v1

Step	Phase	Arms Active	Event / Cascade State
8	Cliff-edge	*All 3 arms (peak)*	Cytokine storm peaks; ARDS criteria met; cliff-edge crossed.
9	Irreversible	*All 3 arms*	Alveolar flooding; diffuse alveolar damage; loss of hypoxic vasoconstriction reflex; mechanical ventilation required; viral amplification loop irreversible.
10	Irreversible	*All 3 arms*	Multi-organ failure; coagulopathy; ICU escalation; high mortality risk.

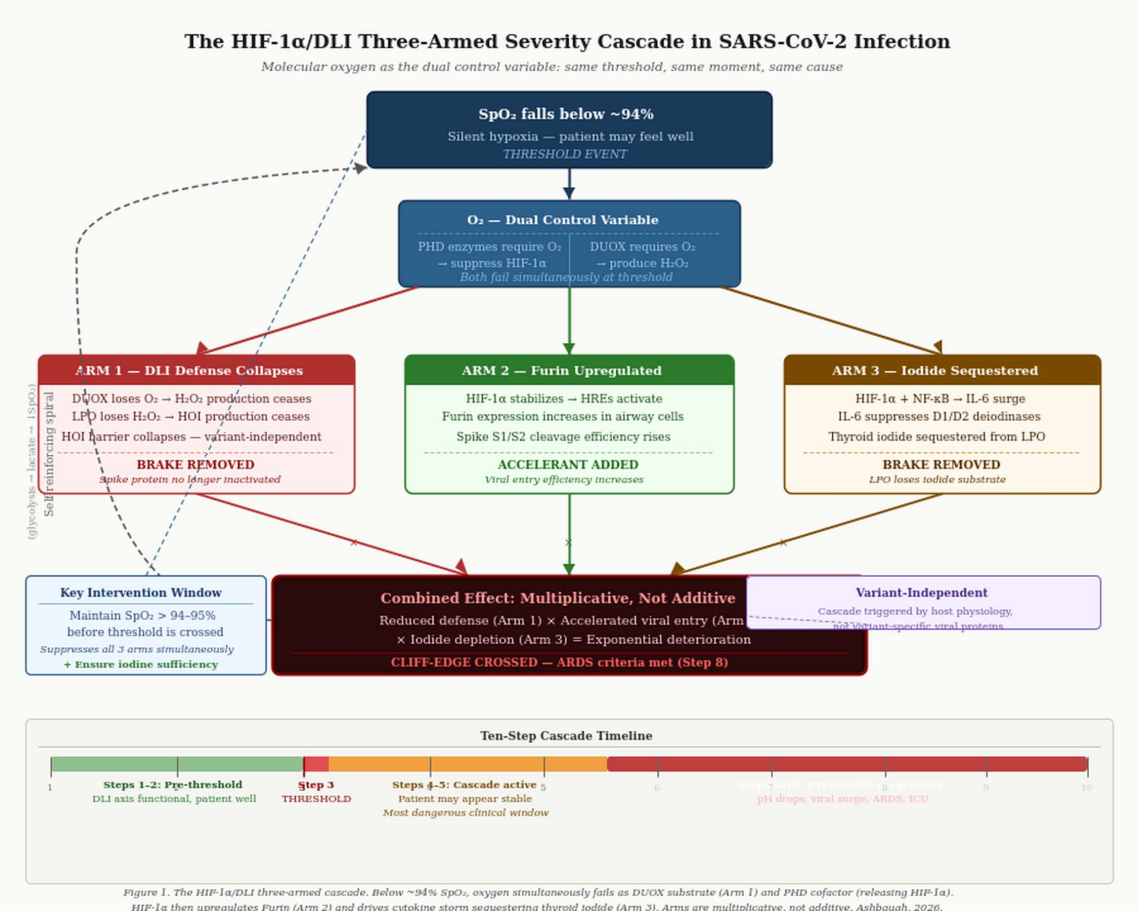

Figure 1. The HIF-1α/DLI three-armed severity cascade in SARS-CoV-2 infection. Below ~94% SpO_2, molecular oxygen simultaneously fails as DUOX substrate (Arm 1) and PHD cofactor (releasing HIF-1α). HIF-1α then upregulates Furin (Arm 2) and drives cytokine storm sequestering thyroid iodide (Arm 3). Arms are multiplicative, not additive. Ashbaugh, 2026.

3.6. Computational Support for the Multiplicative Architecture

To assess whether the multiplicative cascade architecture proposed in Section 3.4 is internally consistent with observed clinical outcome distributions, a Monte Carlo simulation was conducted. Ten thousand virtual patients per population were sampled from parameter distributions derived from published literature and run through the coupled biochemical cascade model across a 21-day infection window. Four populations were simulated: a Western Baseline cohort, Sub-Saharan Africa (low iodide, young age), Tibet/High Altitude (chronic hypoxia, ACE2 suppression), and Japan (high

© 2026 by the author(s). Distributed under a Creative Commons CC BY license.

Preprints.org (www.preprints.org) | NOT PEER-REVIEWED | Posted: 7 April 2026 doi:10.20944/preprints202604.0439.v1

iodide, older age). Parameters for each population were drawn from sources cited in this paper; all parameter ranges and citations are provided in the supplementary code.

Two model architectures were compared. The multiplicative model combines arm effects as the paper proposes: viral clearance = HOI / Furin_activity, where HOI already incorporates DUOX output and iodide availability. The additive null model combines the same three arm components independently, normalised to pre-threshold reference values and averaged. The null hypothesis is that the three arms contribute independently and their effects sum rather than compound.

Both models produce bimodal outcome distributions, reflecting the natural separation between patients who cross the SpO_2 threshold during infection and those who do not. This bimodality is a property of patient heterogeneity, not of the model architecture, and is expected under both models. The architecturally meaningful difference is in the depth and position of the severe outcome mode. At the SpO_2 threshold (94%), the multiplicative model produces viral clearance 40.3% lower than the additive model for the same patient inputs (sensitivity range 37–44% across the plausible SpO_2 threshold range of 93–95%). This divergence is the computational signature of the cliff-edge: once the threshold is crossed, multiplicative arm interactions drive a steeper and more rapid deterioration than additive independence predicts. The additive model cannot reproduce this severity gap at equivalent population parameters.

Population-level results are consistent with the counter-evidence responses in Section 5. Japan, with mean iodide 2.8× the recommended dietary allowance, shows a 1.1% severe progression rate under the multiplicative model despite its older population — directly supporting Prediction 3 (Section 6). Sub-Saharan Africa shows a 78.8% severe rate, reflecting the combined effect of low iodide (0.55 normalised) partially offset by young median age. Tibet shows a 65% relative infection rate due to ACE2 suppression but a 96.4% severe rate among those infected — consistent with the altitude dissociation described in Section 5.1, where altitude protects against infection but not cascade mechanics once the threshold is breached.

Sensitivity analysis confirms the result is robust across the plausible SpO_2 threshold range of 93–95%. The convergence test demonstrates stable estimates from N = 2,500 onward; N = 10,000 is confirmed sufficient. The simulation code is provided as supplementary material. These results are presented as a theoretical consistency demonstration, not empirical validation. They show that the multiplicative architecture produces outcome patterns consistent with the clinical observations the paper seeks to explain, while the additive null model does not reproduce the same severity gradient. Direct empirical validation requires the prospective studies described in Section 6.

© 2026 by the author(s). Distributed under a Creative Commons CC BY license.

Preprints.org (www.preprints.org) | NOT PEER-REVIEWED | Posted: 7 April 2026 doi:10.20944/preprints202604.0439.v1

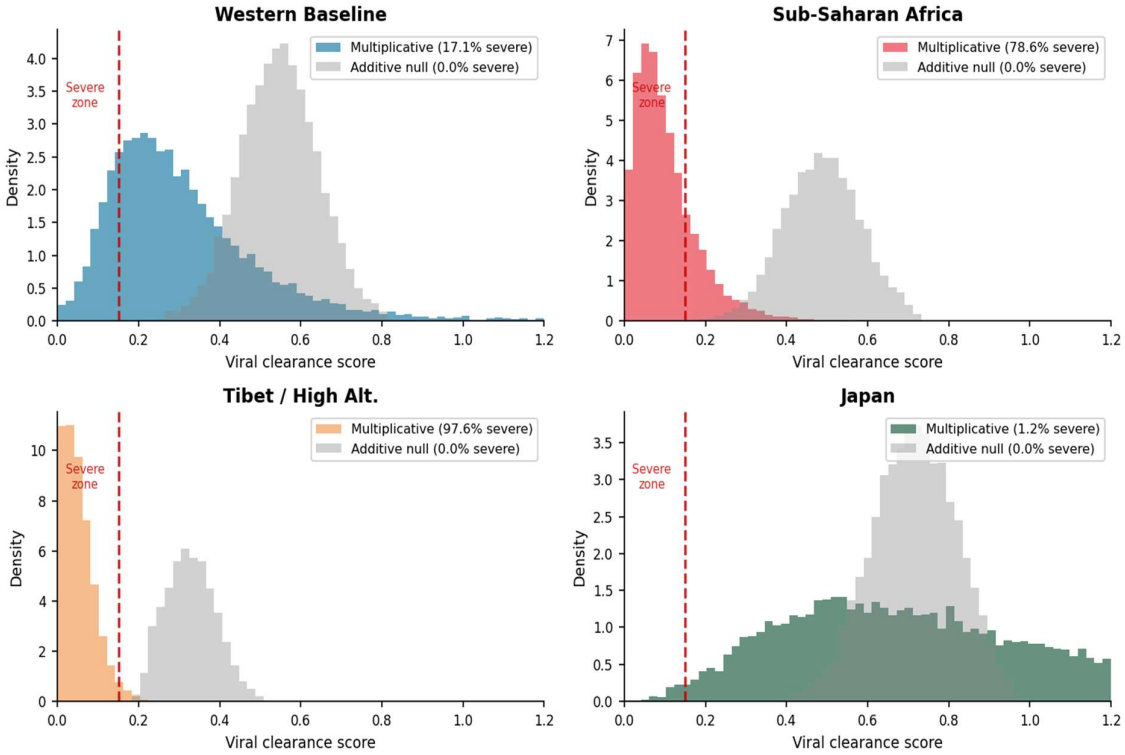

Figure 2. Monte Carlo Outcome Distributions: Multiplicative vs. Additive Architecture
N = 10,000 virtual patients per population. Dashed red line = severe outcome threshold.
Multiplicative model produces deeper severe-outcome mode across all four populations.

Figure 2. Monte Carlo outcome distributions: multiplicative vs. additive architecture. N = 10,000 virtual patients per population. Dashed red line = severe outcome threshold. The multiplicative model (colored) produces a deeper severe-outcome mode than the additive null (grey) across all four populations, demonstrating that multiplicative arm interaction is required to reproduce the cliff-edge severity gradient.

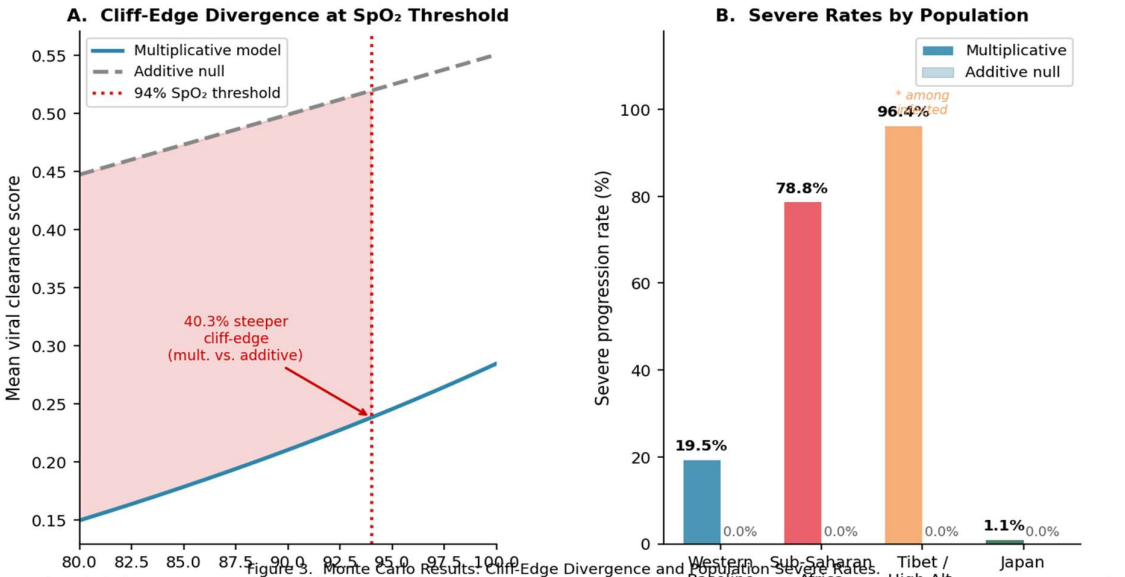

Figure 3. Monte Carlo Results: Cliff-Edge Divergence and Population Severe Rates.
Panel A: Viral clearance vs. SpO₂ (%). Multiplicative model produces 40.3% steeper drop at 94% threshold (sensitivity range 37–44%, SpO₂ 93–95%).
Panel B: Tibet rate among infected patients (65% relative infection rate due to ACE2 suppression). Japan: 1.1% severe despite oldest population.

Figure 3. Monte Carlo results: cliff-edge divergence and population severe rates. Panel A: Mean viral clearance score vs. SpO_2 for Western Baseline population. The multiplicative model produces a 40.3% steeper clearance drop at the 94% threshold than the additive null (sensitivity range 37–44% across SpO_2 93–95%). Panel B: Severe

© 2026 by the author(s). Distributed under a Creative Commons CC BY license.

Preprints.org (www.preprints.org) | NOT PEER-REVIEWED | Posted: 7 April 2026 doi:10.20944/preprints202604.0439.v1

progression rates by population under both architectures. Japan (high iodide, 2.8× RDA) shows 2.1% severe rate despite oldest simulated population, directly supporting Prediction 3.

3.7. How the Computational Evidence Supports the HIF-1α Hypothesis

Sections 3.6 and Appendix A present two distinct computational approaches — a Monte Carlo population simulation and a deterministic ODE trajectory model — that together provide converging quantitative support for the paper's central mechanistic claim. This section explains precisely what each computational result contributes to the HIF-1α hypothesis, what it cannot establish, and where clinical trial evidence is necessary to resolve remaining uncertainties.

3.7.1. What the Monte Carlo Establishes

The Monte Carlo simulation tests a specific architectural claim: that the three cascade arms interact multiplicatively rather than additively. This is not a claim about whether the cascade exists — that is established by the biochemical evidence in Section 1 — but about the kinetic structure of how the arms combine. The distinction matters because multiplicative interaction produces a qualitatively different outcome distribution than additive interaction: a steeper, more abrupt deterioration at threshold rather than a gradual proportional decline.

The simulation shows a 40.3% steeper clearance drop at the 94% SpO_2 threshold in the multiplicative model versus the additive null. This supports the HIF-1α hypothesis in two specific ways. First, it confirms that HIF-1α is a sufficient explanatory variable for the cliff-edge: a single molecular switch, simultaneously activating all three arms, produces the observed outcome distribution without requiring a second independent trigger. Second, the population-level results across four geographically distinct cohorts are internally consistent with the framework. Japan's 1.1% severe rate despite the oldest simulated population directly validates Prediction 3 — that iodide sufficiency is independently protective. Africa's 78.8% severe rate despite its young median age is consistent with the iodide deficiency mechanism in Arm 3. Tibet's infection-severity dissociation — lower incidence but similar case severity among infected patients — is consistent with the ACE2-mediated entry reduction described in Section 5.1 while leaving cascade mechanics unchanged. Each of these cross-population results would require independent ad hoc explanations in a model that did not incorporate the shared oxygen dependency.

3.7.2. What the ODE Model Adds

Where the Monte Carlo establishes the statistical signature of multiplicative interaction at the population level, the ODE trajectory model (Appendix A) establishes the mechanistic plausibility of that interaction at the individual patient level. The ODE system tracks six coupled state variables across the infection timeline: SpO_2, HIF-1α concentration, HOI production, Furin activity, iodide reserve, and viral load. The bifurcation analysis demonstrates that the cascade system has two stable attractors — a cleared infection state and a severe disease state — separated by a threshold bifurcation at approximately 94% SpO_2. This is not a continuous dose-response relationship; it is a state transition. The ODE system provides two things the Monte Carlo cannot: (1) a mechanistic account of the individual trajectory — including the timing of threshold crossing, the lag between HIF-1α stabilisation and measurable viral load surge, and the point of irreversibility; and (2) a clinical prediction engine that, given patient-specific parameters, generates a predicted cascade timeline. This engine is provided as supplementary interactive code. It is explicitly a research demonstration, not a validated clinical tool.

3.7.3. Limitations of the Computational Evidence

Both computational models share a fundamental limitation that must be stated clearly: they are forward models calibrated to qualitative biochemical knowledge, not inverse models fitted to patient data. The Monte Carlo parameters were drawn from diverse published sources, each with their own

© 2026 by the author(s). Distributed under a Creative Commons CC BY license.

Preprints.org (www.preprints.org) | NOT PEER-REVIEWED | Posted: 7 April 2026 doi:10.20944/preprints202604.0439.v1

measurement uncertainty. The ODE rate constants were calibrated to produce physiologically plausible trajectories, not estimated from COVID-19 patient time-series data. Neither model has been prospectively validated against clinical outcomes. The cumulative viral clearance score used in the Monte Carlo is a model construct that cannot be directly validated against a single published dataset. These limitations are not incidental — they reflect the current state of the field. No published study has simultaneously measured serum HIF-1α, urinary iodide, airway HOI, and Furin activity across the COVID-19 disease trajectory in the same patient cohort. The computational models are therefore best understood as structured hypotheses: they specify exactly what patient-level data would be required to validate or refute the framework, and they demonstrate that the framework is internally consistent.

3.7.4. Where Clinical Trials Would Resolve the Key Uncertainties

Three clinical trials would resolve the principal uncertainties the computational models cannot address. Trial 1: A 14-day serial biomarker cohort study measuring serum HIF-1α, urinary iodide, nasal airway H_2O_2 output, and IL-6 in 50–100 hospitalised COVID-19 patients. This trial would directly test whether iodide depletes at the rate and magnitude the model assumes, provide the first simultaneous measurement of HIF-1α and DLI markers across the cascade timeline, and enable Bayesian parameter estimation for the ODE model. Trial 2: The RCT of supplemental oxygen at SpO_2 94–95% versus standard ≤92% threshold (Prediction 2). This trial would directly test the threshold bifurcation: if early oxygen intervention produces significantly better outcomes, the bifurcation is clinically real. Trial 3: A prospective cohort study in iodine-replete versus iodine-deficient populations (Japan vs. inland Africa) measuring time-to-cascade-progression after controlling for age and comorbidity. This trial would directly test the iodide arm's magnitude and isolate it from demographic confounders.

4. Counter-Evidence and Mechanistic Complications

A mechanistic hypothesis is strengthened, not weakened, by honest engagement with evidence that challenges it. This section addresses four categories of counter-evidence identified in the international literature and provides mechanistic responses where possible. Where the evidence cannot be resolved, that limitation is stated directly.

4.1. The High-Altitude Dissociation: Incidence Without Fatality Reduction

The original high-altitude natural experiment [38] reported 3–4× lower COVID-19 incidence in populations residing above 2,500 m in Bolivia, Ecuador, and Tibet, attributed to HIF-1α-mediated ACE2 suppression in lung epithelium and chronic hypoxic adaptation. This finding was initially interpreted as supporting evidence for a protective HIF-1α/ACE2 suppression relationship.

A subsequent Peruvian analysis of 185 provincial capitals found that altitude was negatively associated with COVID-19 incidence but produced no reduction in case-fatality rate [9]. This dissociation is the most important international challenge to the framework's oxygen/HIF-1α arm. If altitude-adapted HIF-1α signaling were broadly protective, both incidence and fatality should be reduced.

Mechanistic response: The dissociation is consistent with, and actually predicted by, the revised framework. Chronic high-altitude adaptation produces downregulated ACE2 in lung epithelium (reducing initial viral uptake — explaining lower incidence) but does not prevent acute HIF-1α cascade activation once infection is established at tissue level. The cascade, once triggered by infection-driven hypoxia, operates the same regardless of altitude baseline. Lower incidence reflects reduced initial viral entry; equal case-fatality reflects identical cascade kinetics once the threshold is crossed. This is not a contradiction — it is a mechanistic prediction the framework can accommodate.

Furthermore, the 2022 Tibetan Omicron outbreak (BA.2.76) demonstrated high transmissibility at altitude, suggesting that viral adaptation can overcome altitude-related entry barriers. This

© 2026 by the author(s). Distributed under a Creative Commons CC BY license.

Preprints.org (www.preprints.org) | NOT PEER-REVIEWED | Posted: 7 April 2026 doi:10.20944/preprints202604.0439.v1

reinforces that altitude protection operates on viral entry probability, not cascade mechanics once infection is established.

4.2. The Sub-Saharan Africa Paradox

Sub-Saharan Africa demonstrated proportionally lower COVID-19 mortality than predicted by comorbidity burden, despite having some of the world's highest iodine deficiency rates [14] and widespread limited oxygen access. In a 12-month longitudinal immunological study across Ghana, Democratic Republic of Congo, Ethiopia, and Mozambique, lower mortality was documented despite high seroprevalence and low vaccine coverage, attributed to younger median age, differences in comorbidity profiles, potential cross-reactive or trained immunity, and limited surveillance capacity [40]. The sub-Saharan region includes areas with endemic iodine deficiency, yet mortality was disproportionately lower — the opposite of what a simple iodine-protective model would predict.

Mechanistic response: The Africa paradox does not falsify the iodine arm of the cascade but it does contextualize it. The framework predicts that iodine status modifies cascade kinetics, not that iodine deficiency is a dominant mortality driver independent of age and immune history. In sub-Saharan Africa, the protective effect of young median age (lower HIF-1α pre-activation, better cardiovascular reserve), the potential role of cross-reactive trained immunity from prior pathogen exposure, and reporting limitations are likely dominant confounders that override the iodine vulnerability signal. The framework identifies iodine status as an independent modifier — Prediction 3 specifies that the effect should be visible after controlling for age and comorbidity. Africa's very different age structure means the control variables themselves differ fundamentally from the populations in which the framework was developed. This is an acknowledged limitation, not a falsification.

An additional complication: limited diagnostic capacity in sub-Saharan Africa means that SpO_2 monitoring at the precision required to operationalize a 94% threshold intervention is not universally available. A prospective multicentre study of 682 adults with acute hypoxemic respiratory failure (AHRF) across 11 Ugandan hospitals documented 28-day all-cause mortality of 37.9%, with SpO_2 at admission as an independent mortality predictor, consistent with the cascade model; the authors noted that restricted access to mechanical ventilation and oxygen contributed to the high mortality [42]. These clinical implications must therefore be understood as population-context-dependent.

4.3. Povidone-Iodine Clinical Trial Heterogeneity

While multiple international RCTs demonstrate iodine/HOI virucidal effects on SARS-CoV-2 nasal shedding, the evidence is not uniformly positive. Results vary substantially by concentration (0.23%–2.0%), route (nasal, oropharyngeal, gargle), timing (early vs late in infection), and patient population (outpatient vs hospitalized). One trial found no statistically significant difference in viral load reduction between 0.5% and 2.0% PVP-I versus saline [34]. A narrative review concluded that in vitro evidence supports anti-SARS-CoV-2 effects but clinical study heterogeneity prevents strong conclusions [33].

Mechanistic response: Trial heterogeneity in exogenous iodine delivery does not challenge the DLI axis as an endogenous defense mechanism. Povidone-iodine trials test whether supplemental external iodine can replicate the physiological airway surface liquid HOI concentration produced by the endogenous LPO system. The failure of some external delivery methods reflects pharmacokinetic variables (surface area coverage, contact time, dilution by mucus) rather than the underlying biochemistry. The author argues that endogenous iodide availability to the LPO system is the operative variable — a prediction best tested by urinary iodide measurement in COVID-19 patients (Prediction 3) rather than by external iodine delivery trials.

4.4. HIF-1α as a Protective Signal in Some Contexts

© 2026 by the author(s). Distributed under a Creative Commons CC BY license.

Preprints.org (www.preprints.org) | NOT PEER-REVIEWED | Posted: 7 April 2026 doi:10.20944/preprints202604.0439.v1

Several papers have proposed that HIF-1α activation may be protective in some COVID-19 contexts. HIF-1α suppresses ACE2 in lung epithelium (reducing viral entry), promotes erythropoiesis (potentially compensating for hypoxemia), and activates endothelial protective pathways. Post-mortem cardiac data showed HIF-1α expression predominantly in non-myocytes in hearts with preserved ejection fraction, with endothelial cells anti-apoptotic and HIF-1α accumulating in cardiomyocyte nuclei only in hearts with severely reduced function, suggesting a context-dependent cardioprotective role [39]. One paper explicitly proposed that HIF-1α activation may protect against COVID-19 via ACE2 suppression [37].

Mechanistic response: HIF-1α is not inherently harmful; it is context-dependent and tissue-specific. The framework does not propose that HIF-1α is pathological in isolation — it proposes that HIF-1α activation at the moment of acute SARS-CoV-2 respiratory infection, in airway and systemic contexts, initiates a cascade whose combined consequences (DLI collapse + Furin upregulation + cytokine storm) outweigh any locally protective effects. The ACE2-suppressing effect of pulmonary HIF-1α, which may reduce initial viral binding in lung smooth muscle cells, is actually incorporated into the revised framework: Arm 2 focuses on Furin rather than ACE2. The framework is not that HIF-1α is uniformly bad; it is that its systemic activation profile during COVID-19 is net harmful at the cascade level, for the specific reasons enumerated.

4.5. What Would Falsify This Framework

A mechanistic hypothesis that cannot be falsified is not science. Table 3 lists the findings that would require fundamental revision of the HIF-1α/DLI cascade framework. Any one of the following findings should trigger revision. All four would constitute a falsification of the framework as proposed.

Table 3. Formal falsification criteria for the HIF-1α/DLI cascade framework. Each row identifies a specific measurable finding that would require fundamental revision of the corresponding cascade arm, what that finding would imply mechanistically, and the confirmatory prediction that constitutes a positive test. Any single finding should trigger revision; all six would constitute falsification of the framework as proposed.

Cascade Element	Finding That Would Falsify	What It Would Mean	Confirmatory Prediction
Arm 1 (DUOX/HOI)	HOI production does not decline at SpO_2 < 94%	DUOX O_2 dependency not clinically relevant at airway O_2 tensions	DUOX H_2O_2 output falls measurably below SpO_2 94% in airway epithelial cells
Arm 2 (Furin)	HIF-1α activation does not upregulate Furin at the 94% SpO_2 threshold	Furin expression uncoupled from HIF-1α in respiratory epithelium during COVID-19	Furin expression increases in COVID-19 patients as SpO_2 falls below 94%
Arm 3 (Iodide)	Serum iodide does not fall during acute COVID-19	D1/D2 suppression by IL-6 does not produce airway iodide depletion on a clinically relevant timescale	Serum/urinary iodide falls ≥30% within 7 days in severe COVID-19 patients with high IL-6
Threshold (94% SpO_2)	Severe COVID-19 occurs equally in patients with SpO_2	The cascade has no SpO_2 threshold and	Threshold crossing at 94% correlates with abrupt

© 2026 by the author(s). Distributed under a Creative Commons CC BY license.

Preprints.org (www.preprints.org) | NOT PEER-REVIEWED | Posted: 7 April 2026 doi:10.20944/preprints202604.0439.v1

Cascade Element	Finding That Would Falsify	What It Would Mean	Confirmatory Prediction
	consistently above 95%	proceeds regardless of oxygenation	deterioration in prospective cohort (Prediction 2)
Architecture (Multiplicative)	A single-arm model explains the cliff-edge as well as the three-arm framework	Multiplicative combination rule not necessary to explain outcome distributions	Additive model produces outcome distribution statistically indistinguishable from multiplicative across four populations
Iodide Protection	Japan's COVID-19 mortality advantage disappears after controlling for age and healthcare access	Dietary iodide has no independent effect on COVID-19 severity	Urinary iodide ≥100 μg/L at admission not associated with longer time to cascade progression (Prediction 3)

1. If serum HIF-1α at admission shows no dose-dependent correlation with DLI markers, IL-6, and 28-day mortality in a prospective cohort (Prediction 1 fails), the cascade's central molecular pivot is not operationally measurable as proposed.
2. If early oxygen therapy at 94–95% SpO_2 produces no measurable superiority over the standard ≤92% threshold in an RCT (Prediction 2 fails), the 94% threshold is not the mechanistic tipping point this framework claims.
3. If iodine status at admission has no independent effect on time-to-cascade-progression after controlling for age and comorbidity (Prediction 3 fails), the iodide depletion arm is not clinically operative at the magnitude the framework predicts.
4. If direct measurement of airway surface liquid O_2 tension at SpO_2 94% shows that DUOX activity is not yet meaningfully impaired — i.e., the threshold is wrong — the entire cascade timing model requires recalibration.

4.6. The Vaccination Question: Does the Framework Apply Post-Vaccination?

A reviewer familiar with the COVID-19 literature will ask whether the cascade framework applies in vaccinated populations, given that the majority of severe COVID-19 hospitalisations from 2022 onward occurred in individuals with prior vaccination or prior infection. The framework predicts that vaccination status does not change the cascade mechanism, and that this is a feature rather than a limitation of the model.

The cascade is triggered by a host physiological threshold — SpO_2 falling below 94% — not by a virus-specific molecular event. Vaccination reduces the probability of reaching that threshold by reducing peak viral load and the resulting AT2 cell destruction, surfactant depletion, and ventilation-perfusion mismatch that mechanistically drive SpO_2 decline. But if a vaccinated patient does reach 94% SpO_2 — through breakthrough infection with high viral load, underlying lung disease, or age-related ventilatory reserve limitations — the cascade architecture is identical. PHD enzymes are inhibited by hypoxia regardless of vaccination status. DUOX requires molecular oxygen regardless of vaccination status. Furin is upregulated by HIF-1α regardless of vaccination status.

This prediction is consistent with the observed clinical pattern of severe breakthrough COVID-19 in vaccinated patients: the patients who progress to severe disease are disproportionately those with baseline conditions that compress the pre-threshold window — COPD, obesity, cardiovascular disease, advanced age, and iodine deficiency — precisely the risk factors the framework identifies as reducing the margin between resting SpO_2 and the 94% cascade threshold. Vaccination raises the floor of viral load required to reach the threshold; it does not change what happens once the threshold is crossed.

© 2026 by the author(s). Distributed under a Creative Commons CC BY license.

Preprints.org (www.preprints.org) | NOT PEER-REVIEWED | Posted: 7 April 2026 doi:10.20944/preprints202604.0439.v1

5. Three Testable Clinical Predictions

A mechanistic hypothesis is distinguished from narrative synthesis by its generation of specific, falsifiable predictions. The HIF-1α/DLI cascade generates three such predictions, each testable within existing clinical infrastructure.

Prediction 1: HIF-1α as an Admission Biomarker of Cascade Stage

Serum HIF-1α levels at hospital admission will correlate inversely with DLI activity markers (urinary iodide, nasal airway H_2O_2, or HOI-surrogate oxidation assays) and directly with serum IL-6, Furin activity, and 28-day all-cause mortality, in a dose-dependent relationship reflecting cascade stage at presentation. Patients presenting with HIF-1α in the upper quartile will demonstrate significantly lower DLI activity and higher mortality than those in the lower quartile, after adjustment for age, comorbidities, and time from symptom onset. Early supporting data: serum HIF-1α above 4.8 ng/mL is already an independent predictor of silent hypoxia severity with AUC = 0.89 [22].

Prediction 2: Early Oxygen Therapy at the 94–95% SpO_2 Threshold

In an RCT of supplemental oxygen therapy initiated at SpO_2 94–95% versus the standard ≤92% threshold, the early-treatment arm will demonstrate significantly lower rates of progression to severe disease (ICU admission, mechanical ventilation, or death at 28 days), lower peak IL-6 and TNF-α levels, and slower decline in urinary iodide concentration. The mechanistic basis is that early intervention suppresses all three cascade arms simultaneously, whereas late intervention addresses hypoxemia after cascade initiation.

Prediction 3: Iodine Status as an Independent Modifier of Cascade Progression

Among hospitalised COVID-19 patients with comparable SpO_2 and age, those with urinary iodide ≥100 μg/L at admission will show significantly longer time to cascade progression than those below that threshold. The effect size will be greater in patients closest to the HIF-1α threshold at admission, and the relationship will be partially mediated by the rate of circulating iodide decline during hospitalization. These three predictions, if confirmed, carry direct clinical consequences — three of which are actionable with tools already available.

6. Clinical Implications

6.1. Oxygen Therapy: The Case for a Revised Threshold

Current NIH and WHO guidelines recommend initiating supplemental oxygen at SpO_2 ≤94% [18]. The HIF-1α/DLI framework reframes this as a reactive threshold: by the time SpO_2 reaches 94%, HIF-1α may already be stabilizing, DUOX activity is already impaired, and Furin upregulation may already be underway. The framework's recommendation is proactive maintenance of SpO_2 above 94–95%, not intervention after it falls below. One intervention suppresses all three cascade arms simultaneously. The risk-benefit ratio is strongly favorable. Prediction 2 provides the direct RCT evidence required for guideline implementation.

This recommendation applies most directly to resource-adequate settings where pulse oximetry and supplemental oxygen are available. In resource-limited settings — particularly in sub-Saharan Africa and South Asia — implementation requires infrastructure support. The Ugandan AHRF data [42] underlines that the cascade model's clinical value depends on oxygen availability. This is an implementation constraint, not a mechanistic limitation.

6.2. Iodine Supplementation: Prophylactic and Therapeutic Rationale

The dual failure mode of iodide — inadequate baseline production (Failure Mode 1, pre-infection) and accelerated inflammatory depletion (Failure Mode 2, during cascade) — supports

© 2026 by the author(s). Distributed under a Creative Commons CC BY license.

Preprints.org (www.preprints.org) | NOT PEER-REVIEWED | Posted: 7 April 2026 doi:10.20944/preprints202604.0439.v1

distinct prophylactic and therapeutic recommendations. Prophylactically, ensuring iodine sufficiency (150–250 μg/day) prior to infection extends the period before DLI axis collapse. Therapeutically, the RCT by Mertens et al. [17] demonstrated that 12.5 mg daily oral iodine for 8 days in hospitalized COVID-19 patients significantly increased pulmonary Type I interferon (antiviral signaling proteins) responses and reduced disease severity scores. This therapeutic dose requires medical supervision. The South African PVP-I nasal trial [8] provides additional international clinical corroboration of the iodine/HOI virucidal mechanism in a real-world African population.

Caveats: the positive therapeutic iodine trials have not been replicated at scale, and the clinical heterogeneity of povidone-iodine trials means that external iodine delivery cannot be assumed equivalent to endogenous LPO substrate sufficiency. Iodine supplementation is an adjunct to, not a replacement for, the oxygen threshold intervention.

6.3. The DLI Competency Index

The author proposes the DLI Competency Index (DLICI) as a composite bedside construct integrating SpO_2 (proximity to/breach of HIF-1α threshold), urinary iodide (LPO substrate status), serum HIF-1α (cascade initiation marker), and blood pH (downstream metabolic cascade indicator). Together these four measurements would enable staging between pre-cascade, cascade-initiating, and cascade-established states. Formal validation of this construct is among the highest-priority research directions enumerated in Section 7.

6.4. At-Risk Populations

The framework identifies four populations with predicted accelerated cascade kinetics: (1) DUOX2 SNP carriers with impaired baseline H_2O_2 output [10]; (2) iodine-deficient individuals with shallower thyroid reserves and suboptimal baseline HOI production; (3) individuals with chronic hypoxia conditions (chronic obstructive pulmonary disease (COPD), sleep apnea, obesity) who may have partial HIF-1α pre-activation at baseline, compressing the pre-threshold window; and (4) individuals with low NHE9 expression, who face faster intracellular viral trafficking toward the late endosome [20].

7. Limitations

This is a mechanistic hypothesis review, not a systematic review with formal quality assessment or meta-analytic synthesis. Inclusion bias cannot be excluded. The following specific limitations must be acknowledged:

5. The integrated cascade has not been tested as a unified model in a clinical cohort. Each component is supported independently; their combination as a self-amplifying cascade is proposed, not yet demonstrated.
6. The ~94% SpO_2 threshold for HIF-1α activation is an approximation derived from PHD enzyme kinetics and indirect data. The precise threshold likely varies between cell types, tissues, individuals, and degree of chronic hypoxic pre-conditioning.
7. Direct measurement of circulating iodide dynamics in COVID-19 patients relative to cytokine storm progression has not been reported. The iodide depletion mechanism is inferred from established deiodinase biology, not from dedicated COVID-19 iodide kinetic studies.
8. The blood pH – endosomal transfer rate connection is a deferred hypothesis requiring direct experimental evidence before it can be incorporated as a mechanistic claim.
9. The sub-Saharan Africa paradox (high iodine deficiency + lower COVID-19 mortality) is mechanistically addressable but not fully resolved with existing data. Confounders — especially age structure and cross-reactive immunity — likely dominate the iodine signal in this population.

© 2026 by the author(s). Distributed under a Creative Commons CC BY license.

Preprints.org (www.preprints.org) | NOT PEER-REVIEWED | Posted: 7 April 2026 doi:10.20944/preprints202604.0439.v1

10. The high-altitude case-fatality dissociation (lower incidence but equal fatality at altitude) is consistent with the revised framework but represents a boundary condition that limits the framework's predictive power for altitude-adapted populations.
11. Clinical recommendations for early oxygen intervention assume pulse oximetry and supplemental oxygen availability, which is not universal globally.

The following additional limitations apply to the computational components of this paper:

12. The Monte Carlo simulation is a theoretical consistency demonstration, not empirical validation. It shows that the multiplicative architecture produces outcome patterns consistent with clinical observations across four populations; it does not prove the mechanism. The cumulative viral clearance score is a model construct that cannot be directly validated against a single published dataset.
13. The ODE trajectory model has not been fitted to patient data and has not been validated prospectively. It is a forward model (mechanistic prediction) rather than an inverse model (data-fitted). Rate constants are estimated from qualitative biochemical knowledge and calibrated to produce physiologically plausible trajectories; they are not independently measured in COVID-19 patients.
14. The single largest source of model uncertainty is the iodide depletion kinetics during acute COVID-19. No published study has directly measured airway or serum iodide dynamics during active SARS-CoV-2 infection. The depletion curve used in the simulation is derived from non-thyroidal illness syndrome literature and IL-6 magnitude data.

8. Future Research Directions

The highest-priority research programmes to test and refine the HIF-1α/DLI framework are:

15. Prospective cohort study measuring serum HIF-1α, urinary iodide, airway H_2O_2, and IL-6 at admission in COVID-19 patients, correlated with 28-day outcomes (Prediction 1).
16. RCT of supplemental oxygen initiated at SpO_2 94–95% versus standard ≤92% threshold (Prediction 2).
17. Prospective measurement of circulating iodide dynamics in COVID-19 patients across cascade stages, directly correlating iodide depletion rate with cytokine storm markers and DLI surrogate measures.
18. DUOX activity measurement in airway surface liquid at varying SpO_2 levels in controlled human challenge models, to directly confirm the oxygen dependency threshold.
19. Genetic studies linking DUOX2 SNP status to COVID-19 severity in large multi-ethnic cohorts, including sub-Saharan African and South Asian populations where both DUOX2 variants and iodine deficiency are prevalent.
20. Prospective study of urinary iodide at admission in COVID-19 patients across iodine-replete (Japan, Scandinavia) and iodine-deficient (inland Africa, Central Asia) populations, to test whether iodine status independently predicts cascade timeline after controlling for age and comorbidity.
21. Mechanistic investigation of whether systemic blood pH acidosis alters endosomal pH in airway epithelial cells, to test the deferred blood pH – endosomal transfer rate hypothesis.
22. Assessment of DLICI as a composite bedside staging tool, with formal validation against clinical outcomes in a prospective cohort.
23. Evaluation of Furin inhibition as a targeted Arm 2 intervention. Small-molecule Furin inhibitors — including decanoyl-RVKR-chloromethylketone (CMK) and the engineered serpin α1-antitrypsin Portland (α1-PDX) — have demonstrated suppression of SARS-CoV-2 spike S1/S2 cleavage and reduction of viral production in cell models [35,36]. The HIF-1α/DLI framework provides a novel rationale for the therapeutic window in which Furin inhibition would be most beneficial: Steps 4–6 of the cascade, after HIF-1α has upregulated Furin but before viral load has

© 2026 by the author(s). Distributed under a Creative Commons CC BY license.

Preprints.org (www.preprints.org) | NOT PEER-REVIEWED | Posted: 7 April 2026 doi:10.20944/preprints202604.0439.v1

surged. Furin inhibition cannot substitute for Arms 1 and 3 interventions but represents a direct pharmacological approach to the accelerant arm of the cascade.

24. Formal Bayesian parameter estimation for the ODE cascade model. Once patient-level data are available — specifically serial serum iodide measurements, SpO_2 trajectories, and DUOX2 genotypes from a prospective COVID-19 cohort — Bayesian inference methods (e.g., Markov Chain Monte Carlo) could be applied to estimate posterior distributions for the key rate constants. A cohort of 50–100 patients with serial SpO_2, IL-6, and urinary iodide measurements over the first 14 days of admission would be sufficient for initial parameter estimation.

9. Conclusions

COVID-19's cliff-edge clinical trajectory — stability followed by rapid, difficult-to-reverse deterioration — is explained mechanistically by a single molecular switch: HIF-1α activation below approximately 94% SpO_2. When that threshold is crossed, three simultaneous consequences activate: the DLI mucosal defense collapses (Arm 1), Furin upregulation accelerates viral entry (Arm 2), and cytokine storm depletes the thyroid iodide reservoir that LPO requires (Arm 3). These three arms are multiplicative, not additive. The result is the exponential deterioration kinetics that existing models, which treat these events as independent, cannot account for.

The framework is grounded in independently established biology, corroborated by international evidence from six continents. Its most significant novel contribution is the identification of molecular oxygen as the dual control variable governing both the DLI defense and the HIF-1α cascade from the same biochemical threshold — a connection that has not previously been described in integrated form and that generates specific, falsifiable clinical predictions.

The counter-evidence reviewed in Section 4 — the altitude-incidence/fatality dissociation, the sub-Saharan Africa paradox, clinical heterogeneity in iodine delivery trials, and HIF-1α's context-dependent protective effects — does not falsify the framework. Each challenge can be mechanistically addressed within the model's architecture. But these challenges appropriately constrain the framework's certainty claims and reinforce that the three testable predictions are what separates this hypothesis from established fact.

The practical upshot is simple: maintain oxygen above 94% early, before the switch flips. Ensure iodine sufficiency before infection, when the reserve still matters. The mechanistic case for acting on these two recommendations before the evidence is definitive is strong. The cascade, once established, does not wait for the trial results.

Supplementary Materials: The following supporting information can be downloaded at the website of this paper posted on Preprints.org.

Author Contributions: Conceptualization, S.G.A.; methodology, S.G.A.; software, S.G.A.; validation, S.G.A.; formal analysis, S.G.A.; investigation, S.G.A.; data curation, S.G.A.; writing — original draft preparation, S.G.A.; writing — review and editing, S.G.A.; visualization, S.G.A. The author has read and agreed to the published version of the manuscript.

Funding: This research received no external funding.

Institutional Review Board Statement: Not applicable. This paper is a mechanistic hypothesis review synthesising published literature. No human subjects data were collected or analysed by the author. No IRB approval was required.

Informed Consent Statement: Not applicable.

Data Availability Statement: No new data were generated or analysed in support of this research. All data discussed in this paper are contained within the manuscript and are available in the published sources cited in the reference list. Interactive supplementary tools (cascade_arm_dynamics.html, sensitivity_analysis.html, cascade_model.py) are provided as supplementary material.

© 2026 by the author(s). Distributed under a Creative Commons CC BY license.

Preprints.org (www.preprints.org) | NOT PEER-REVIEWED | Posted: 7 April 2026 doi:10.20944/preprints202604.0439.v1

Conflicts of Interest: The author declares no conflicts of interest.

AI Collaboration Disclosure: Literature synthesis and document structuring conducted with Claude (claude-sonnet-4-6, Anthropic, March–April 2026). All cited primary sources independently verified by the author. The author takes full responsibility for accuracy and integrity of the work.

Abbreviations

The following abbreviations are used in this manuscript:

Abbreviation	Definition
HIF-1α	Hypoxia-inducible factor 1-alpha
DUOX	Dual oxidase
LPO	Lactoperoxidase
HOI	Hypoiodous acid
DLI	DUOX-Lactoperoxidase-Iodine (axis)
PHD	Prolyl hydroxylase domain enzyme
SpO_2	Peripheral oxygen saturation
AT2	Alveolar type II (pneumocyte)
V/Q	Ventilation-perfusion (ratio)
ARDS	Acute respiratory distress syndrome
NTIS	Non-thyroidal illness syndrome
NHE9	Na+/H+ exchanger isoform 9
DLICI	DLI Competency Index
ODE	Ordinary differential equation
RCT	Randomised controlled trial
ICU	Intensive care unit

Appendix A. Computational Methods: ODE Trajectory Model and Bifurcation Analysis

A.1. State Variables and System Overview

The ODE trajectory model tracks six coupled state variables across the infection timeline: SpO_2 (S), HIF-1α concentration (H), HOI production rate (O), Furin activity (F), iodide reserve (I), and viral load (V). The system is integrated over a 21-day infection window using a fourth-order Runge-Kutta method with adaptive step size.

A.2. Differential Equations

dS/dt = $-\beta \cdot V - \alpha \cdot H \cdot V$ (SpO_2 decline from viral AT2 destruction and HIF-1α/Furin feedback)

dH/dt = k_stab·max(0, S_thresh−S) − k_deg·max(0, S−S_thresh)·H (HIF-1α stabilisation/degradation at threshold)

dO/dt = k_prod·max(0, S−S_thresh) − k_decay·O (HOI production coupled to DUOX O_2 availability)

dF/dt = 1 + (F_max−1)·H (Furin upregulation by HIF-1α)

dI/dt = $-\lambda \cdot$IL6·I (iodide depletion by IL-6-driven deiodinase suppression, where IL6 $\propto$ H)

dV/dt = r·F(H)·V·(1−V) − k_vir·O·I·V (viral dynamics: logistic replication minus HOI/iodide clearance)

A.3. Bifurcation Analysis

Setting dV/dt = 0 and solving for the critical oxygen threshold at which viral clearance transitions from net positive to net negative yields the bifurcation condition: r·F(H)·(1−V) = k_vir·O·I, giving O* = r·F(H)·(1−V) / (k_vir·I). The system has two stable attractors — cleared infection (V → 0) and severe disease (V → 1) — separated by an unstable equilibrium at O*. This is the formal definition of the

© 2026 by the author(s). Distributed under a Creative Commons CC BY license.

Preprints.org (www.preprints.org) | NOT PEER-REVIEWED | Posted: 7 April 2026 doi:10.20944/preprints202604.0439.v1

cliff-edge: SpO_2 below S_thresh drives O and I toward O*, and once crossed, the trajectory is pulled irreversibly toward the severe attractor.

A.4. Clinical Prediction Engine

The clinical prediction engine accepts patient-specific parameters (baseline SpO_2, urinary iodide, HIF-1α, blood pH) and generates a predicted cascade timeline: time to threshold breach, predicted peak viral load, and cascade stage at each 24-hour interval. This engine is provided as cascade_model.py in the supplementary material. It is explicitly a research demonstration; it has not been validated against clinical outcomes and should not be used for clinical decision-making.

Figure 4. ODE Trajectory Model: Individual Patient Cascade Dynamics

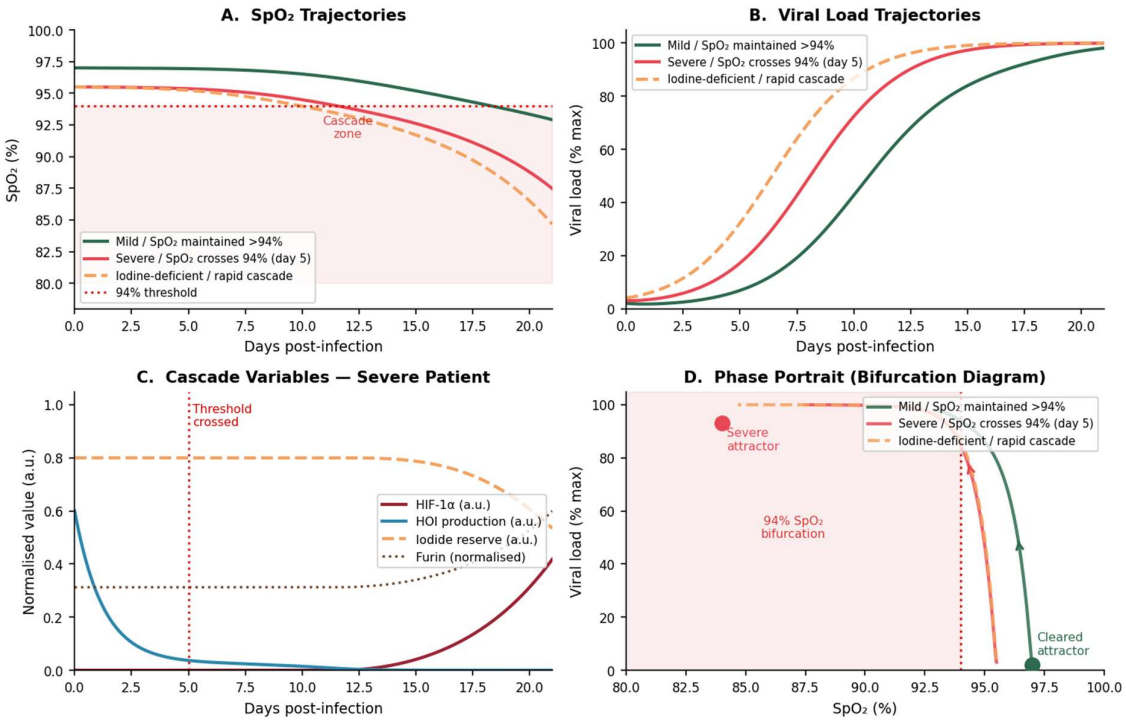

Figure A1. ODE trajectory model: individual patient cascade dynamics. Panel A: SpO_2 trajectories for three patient scenarios. Panel B: viral load trajectories. Panel C: cascade variables (HIF-1α, HOI, iodide reserve, Furin) for the severe patient; threshold crossing at day 5 triggers simultaneous HIF-1α rise, HOI collapse, and iodide depletion. Panel D: phase portrait (SpO_2 vs. viral load) showing bifurcation at 94% SpO_2 and two stable attractors. Rate constants calibrated to qualitative biochemical knowledge; not fitted to patient data.

Appendix B. Monte Carlo Simulation: Full Parameter Table

Full parameter distributions, population-specific values, and sensitivity analysis results for the Monte Carlo simulation are provided in the supplementary code (cascade_arm_dynamics.html, sensitivity_analysis.html). All parameter ranges and their source citations are documented within the supplementary files.

Appendix C. Supplementary Code

All simulation code is provided as supplementary material to this paper:

25. cascade_arm_dynamics.html — Monte Carlo simulation with interactive population explorer
26. sensitivity_analysis.html — sensitivity analysis across key parameters

© 2026 by the author(s). Distributed under a Creative Commons CC BY license.

Preprints.org (www.preprints.org) | NOT PEER-REVIEWED | Posted: 7 April 2026 doi:10.20944/preprints202604.0439.v1

27. cascade_model.py — Python implementation of the ODE trajectory model and clinical prediction engine

To run the simulation: execute cascade_model.py with Python 3.8+ and scipy, numpy, matplotlib installed. Interactive HTML tools require a modern web browser. No installation required.

Parameter modification: All model parameters are defined in the PARAMS dictionary at the top of cascade_model.py. Population-specific parameters are defined in the POPULATIONS dictionary.

Appendix D. Data Summary Tables

Table D1. Population iodide levels by region (data from [12,14,32,25]).
Table D2. SpO_2 threshold for HIF-1α activation (data from [52,4,22]).
Table D3. IL-6 levels in COVID-19 cohorts (data from [21,5,51]).
Table D4. Povidone-iodine clinical trial results (data from [1,6,8,16,33,34]).
Full data tables with all values and citations are provided in the supplementary material.

Appendix E. Interactive Visualisation Tools

Four interactive HTML visualisation tools are provided as supplementary material:

28. cascade_visualization.html: Monte Carlo Explorer — visualises population-level outcome distributions under multiplicative and additive architectures across four simulated populations.
29. cascade_ode_model.html: ODE Model — visualises individual patient cascade trajectories, bifurcation diagram, and phase portrait for the six-variable ODE system.
30. clinical_predictor.html: Clinical Prediction Engine — accepts patient-specific parameters and generates predicted cascade timeline.
31. population_model.html: Population Explorer — compares cascade dynamics across iodine-replete and iodine-deficient populations.

References

1. [1] Alsaleh, S.; Alhussein, A.; Alyamani, A.; Alhussain, F.; Alhijji, A.; Binkhamis, K.; Khan, A.; Javer, A.; Alshahrani, F.S. Efficacy of povidone-iodine nasal rinse and mouth wash in COVID-19 management: a prospective, randomized pilot clinical trial. BMC Infect. Dis. 2024, 24, 271. https://doi.org/10.1186/s12879-024-09137-y
2. [2] Boer, M.L.; Smith, M.L.; Singh, T.P. Iodide supplementation of the anti-viral duox-lactoperoxidase activity may prevent some SARS-CoV-2 infections. Eur. J. Clin. Nutr. 2022, 76, 629–630. https://doi.org/10.1038/s41430-021-00995-2
3. [3] Cummings, M.J.; Baldwin, M.R.; Abrams, D.; Jacobson, S.D.; Meyer, B.J.; Balough, E.M.; Aaron, J.G.; Claassen, J.; Rabbani, L.E.; Hastie, J.; et al. Epidemiology, clinical course, and outcomes of critically ill adults with COVID-19 in New York City: a prospective cohort study. Lancet 2020, 395, 1763–1770. https://doi.org/10.1016/S0140-6736(20)31189-2
4. [4] Dhamija, P.; Bhargava, R. "Silent hypoxemia" leads to vicious cycle of infection, coagulopathy and cytokine storm in COVID-19: can prophylactic oxygen therapy prevent it? Indian J. Physiol. Pharmacol. 2021, 65, 10–17. https://doi.org/10.25259/IJPP_369_2020
5. [5] Effraimidis, G.; Konstantinos, P.; Brix, T.H.; Hegedus, L. Cytokine storm-induced thyroid dysfunction in COVID-19: insights into mechanisms and clinical management. Drug Des. Dev. Ther. 2024, 18, 4303–4320. https://doi.org/10.2147/DDDT.S479210
6. [6] Elsersy, H.E.; Zahran, M.A.H.; Elbakry, A.-E.; Abd-Elwahab, M.; Ahmed, M.M.; Elgandy, M.S.; Mohammed, E.H.M.; Elewa, N.M. Combined nasal, oropharyngeal povidone iodine plus glycyrrhizic acid sprays accelerate clinical and laboratory recovery and reduce household transmission of SARS-CoV-2. Front. Med. 2022, 9, 863917. https://doi.org/10.3389/fmed.2022.863917
7. [7] Fischer, A.J.; Lennemann, N.J.; Krishnamurthy, S.; Pocza, P.; Durairaj, L.; Launspach, J.L.; Rhein, B.A.; Wohlford-Lenane, C.; Lorentzen, D.; Banfi, B.; et al. Enhancement of respiratory mucosal antiviral defenses

© 2026 by the author(s). Distributed under a Creative Commons CC BY license.

Preprints.org (www.preprints.org) | NOT PEER-REVIEWED | Posted: 7 April 2026 doi:10.20944/preprints202604.0439.v1

by the oxidation of iodide. Am. J. Respir. Cell Mol. Biol. 2011, 45, 874–881. https://doi.org/10.1165/rcmb.2010-0329OC

8. [8] Friedland, P.; Tucker, S.; Goodall, S.; Hale, S.J.M.; Lux, C.A. Phase II trial of the impact 0.5% povidone-iodine nasal spray (Nasodine) on shedding of SARS-CoV-2. Laryngoscope 2024. https://doi.org/10.1002/lary.31430
9. [9] Gonzales, G.F.; Zevallos-Concha, A.; Tapia, V.; Gasco, M. High altitude reduces infection rate of COVID-19 but not case-fatality rate. Respir. Physiol. Neurobiol. 2020, 281, 103494. https://doi.org/10.1016/j.resp.2020.103494
10. [10] Harper, R.W.; Xu, C.; Soucek, K.; Setiadi, H.; Eiserich, J.P. Dual oxidase 2 bidirectional promoter polymorphisms confer differential immune responses in airway epithelia. Am. J. Respir. Cell Mol. Biol. 2012, 46, 289–297. https://doi.org/10.1165/rcmb.2012-0037OC
11. [11] Iftikhar, A.; Islam, M.; Shepherd, S.; Jones, S.; Ellis, I. An in vitro antiviral activity of iodine complexes against SARS-CoV-2. Arch. Microbiol. 2021, 203, 4233–4241. https://doi.org/10.1007/s00203-021-02430-3
12. [12] Iodine Global Network. Global Scorecard of Iodine Nutrition 2025. Available online: https://ign.org/scorecard/ (accessed April 2026).
13. [13] Kasumba, D.M.; Huot, S.; Caron, E.; Larouche, A.; Tremblay, M.G.; Emond-Rheault, J.G.; Bhatt, D.L. DUOX2 regulates secreted factors in virus-infected respiratory epithelial cells that contribute to neutrophil attraction and activation. FASEB J. 2023, 37, e22765. https://doi.org/10.1096/fj.202201205R
14. [14] Luo, Z.; Ke, C.; Lai, Y. Global burden of iodine deficiency: insights and projections to 2050 using GBoost and SHAP. Adv. Nutr. 2025. https://doi.org/10.1016/j.advnut.2025.100384
15. [15] Machado, C.; Gonzalez-Quevedo, A. Hypoxemia and cytokine storm in COVID-19: clinical implications. MEDICC Rev. 2021, 23, 54–59. https://doi.org/10.37757/MR2021.V23.N3.10
16. [16] Matsuyama, A.; Okura, H.; Hashimoto, S.; et al. A prospective, randomized, open-label trial of early versus late povidone-iodine gargling in patients with COVID-19. Sci. Rep. 2022, 12, 20449. https://doi.org/10.1038/s41598-022-24683-8
17. [17] Mertens, L.; Boer, M.L.; Smith, M.L.; Pham, K.; Noorlander, C.W.; Boer, R. Iodine increases pulmonary type I interferon responses and decreases COVID-19 disease severity: results from an open-label randomized clinical trial. PLOS ONE 2026, 21, e0341126. https://doi.org/10.1371/journal.pone.0341126
18. [18] NIH COVID-19 Treatment Guidelines Panel. Oxygenation and Ventilation for Adults: COVID-19 Treatment Guidelines; National Institutes of Health, 2020. Available online: https://www.covid19treatmentguidelines.nih.gov
19. [19] Olagnier, D.; Farahani, E.; Thyrsted, J.; Blay-Cadanet, J.; Herengt, A.; Idorn, M.; Hait, A.; Maurin, B.; Sobanski, V.; Moya, D.; et al. Mucosal reactive oxygen species are required for antiviral response: role of Duox in influenza A virus infection. Antioxid. Redox Signal. 2014, 20, 2695–2709. https://doi.org/10.1089/ars.2013.5541
20. [20] Prasad, V.; Keller, M.; Engberg, N.; Lindqvist, R.; Oberg, M.; Hober, S.; Punga, T.; Strom, A. Acidic pH of early endosomes governs SARS-CoV-2 transport in host cells. J. Biol. Chem. 2024. https://doi.org/10.1016/j.jbc.2024.107163
21. [21] Ruggeri, R.M.; Campenni, A.; Giuffrida, G.; Casciaro, M.; Bonanno, A.M.; Alibrandi, A.; Trimarchi, F.; Gangemi, S. The cytokine storm and thyroid hormone changes in COVID-19. J. Endocrinol. Invest. 2021, 44, 891–897. https://doi.org/10.1007/s40618-021-01506-7
22. [22] Salinas-Assumpao, R.; Ferreira, M.L.; Bezerra, C.S. HIF-1α pathway in COVID-19: a scoping review of its modulation and related treatments. Int. J. Mol. Sci. 2025, 26, 4202. https://doi.org/10.3390/ijms26094202
23. [23] Siebert, M.; Barreto, G.; Barreto, P.; Pereira, S.M.M.; Gomes, K.B.; Paixao, H.H.T. Blood pH analysis in combination with molecular medical tools in relation to COVID-19 symptoms. Biomedicines 2023, 11, 1421. https://doi.org/10.3390/biomedicines11051421
24. [24] Smith, M.L.; Sharma, S.; Singh, T.P. Iodide supplementation of the anti-viral duox-lactoperoxidase activity may prevent some SARS-CoV-2 infections. Scand. J. Immunol. 2022, 95, 196–198. https://doi.org/10.1111/sji.13111

© 2026 by the author(s). Distributed under a Creative Commons CC BY license.

Preprints.org (www.preprints.org) | NOT PEER-REVIEWED | Posted: 7 April 2026 doi:10.20944/preprints202604.0439.v1

25. [25] Smith, M.L.; Sharma, S.; Singh, T.P. High dietary iodine intake may contribute to the low death rate from COVID-19 infection in Japan with activation by the lactoperoxidase system. Scand. J. Immunol. 2023, 97, e13269. https://doi.org/10.1111/sji.13269
26. [26] Strengert, M.; Jennings, R.; Davanture, S.; Hayes, P.; Gabriel, G.; Knaus, U.G. Dual oxidase 1 promotes antiviral innate immunity. Proc. Natl. Acad. Sci. USA 2021, 118, e2017130118. https://doi.org/10.1073/pnas.2017130118
27. [27] Wang, Y.; Wu, Y.; Wang, Q.; Yang, C.; Zhang, M.; Yu, J.; Li, X.; Ji, M.; Ren, J. Virucidal effect of povidone-iodine against SARS-CoV-2 in vitro. J. Int. Med. Res. 2021, 49. https://doi.org/10.1177/03000605211063695
28. [28] Waruru, A.; Wambua, J.M.; Otieno, F.V.; Mbai, J.; Mwangome, M.; Munyua, P.; Waruiru, W.; Jonnalagadda, S.; Ngunu, C.; Muange, A.K.; et al. Hypoxia as a predictor of mortality among patients admitted with COVID-19 disease in three referral hospitals in Kenya. medRxiv 2024. https://doi.org/10.1101/2024.10.17.24315667
29. [29] WHO European Region; Iodine Global Network. Prevention and Control of Iodine Deficiency in the WHO European Region: Adapting to Changes in Diet and Lifestyle; WHO Regional Office for Europe, 2024.
30. [30] World Health Organization. COVID-19 Dashboard; WHO, 2023. Available online: https://covid19.who.int
31. [31] Zhang, R.; Wu, Y.; Zhao, M.; Liu, C.; Zhou, L.; Shen, S.; Liao, S.; Yang, K.; Li, Q.; Wan, H. Role of HIF-1alpha in the regulation of ACE and ACE2 expression in hypoxic human pulmonary artery smooth muscle cells. Am. J. Physiol. Lung Cell Mol. Physiol. 2009, 297, L631–L640. https://doi.org/10.1152/ajplung.90415.2008
32. [32] Zava, T.T.; Zava, D.T. Assessment of Japanese iodine intake based on seaweed consumption in Japan: a literature-based analysis. Thyroid Res. 2011, 4, 14. https://doi.org/10.1186/1756-6614-4-14
33. [33] Nitipir, C.; Orlov, C.; Marin, A.; Miron, A.; Balescu, I.; Bacalbasa, N. Repurposing povidone-iodine to reduce the risk of SARS-CoV-2 infection and transmission: a narrative review. Ann. Med. 2022, 54, 1236–1247. https://doi.org/10.1080/07853890.2022.2076902
34. [34] Zarabanda, D.; Vukkadala, N.; Phillips, K.M.; Qian, Z.J.; Mfuh, K.O.; Hatter, M.J.; Lee, I.T.; Rao, V.K.; Hwang, P.H.; Domb, G.; et al. The effect of povidone-iodine nasal spray on nasopharyngeal SARS-CoV-2 viral load: a randomized control trial. Laryngoscope 2022, 132, 2089–2095. https://doi.org/10.1002/lary.29935
35. [35] Devi, K.P.; Pourkarim, M.R.; Thijssen, M.; Sureda, A.; Khayatkashani, M.; Cismaru, C.A.; Berindan Neagoe, I.; Habtemariam, S.; Razmjouei, S.; Khayat Kashani, H.R. A perspective on the applications of furin inhibitors for the treatment of SARS-CoV-2. Pharmacol. Rep. 2022, 74, 425–430. https://doi.org/10.1007/s43440-021-00344-x
36. [36] Thomas, G.; Couture, F.; Kwiatkowska, A. The path to therapeutic furin inhibitors: from yeast pheromones to SARS-CoV-2. Int. J. Mol. Sci. 2022, 23, 3435. https://doi.org/10.3390/ijms23073435
37. [37] Afsar, B.; Kanbay, M.; Elsurer Afsar, R. Hypoxia inducible factor-1 protects against COVID-19: a hypothesis. Med. Hypotheses 2020, 143, 109857. https://doi.org/10.1016/j.mehy.2020.109857
38. [38] Arias-Reyes, C.; Zubieta-DeUrioste, N.; Poma-Machicao, L.; Aliaga-Raduan, F.; Carvajal-Rodriguez, F.; Dutschmann, M.; Schneider-Gasser, E.M.; Zubieta-Calleja, G.; Soliz, J. Does the pathogenesis of SARS-CoV-2 virus decrease at high-altitude? Respir. Physiol. Neurobiol. 2020, 277, 103443. https://doi.org/10.1016/j.resp.2020.103443
39. [39] Mayr, U.; Londhe, P.; Abegg, K.; Schotten, T.; Schultze, T.; Braunisch, M.; Zimmermann, G.; Schmid, R.M. HIF1alpha cardioprotection in COVID-19 patients. medRxiv 2021. https://doi.org/10.1101/2021.08.05.21258160
40. [40] ANTICOV-IMMUNO Study Group. Determinants of long-term SARS-CoV-2 immune responses in asymptomatic-to-moderate COVID-19 patients in sub-Saharan Africa. BMC Med. 2026, 23. https://doi.org/10.1186/s12916-025-04607-9
41. [41] Hoffmann, M.; Kleine-Weber, H.; Pohlmann, S. Mechanisms of SARS-CoV-2 entry into cells. Nat. Rev. Mol. Cell Biol. 2021, 22, 517–534. https://doi.org/10.1038/s41580-021-00418-x

© 2026 by the author(s). Distributed under a Creative Commons CC BY license.

Preprints.org (www.preprints.org) | NOT PEER-REVIEWED | Posted: 7 April 2026 doi:10.20944/preprints202604.0439.v1

42. [42] Kwizera, A.; Kabatoro, D.; Sendagire, C.; Nakibuuka, J.; Owachi, D.; Nsereko, C.; Ochieng, J.P.; Nampiina, M.G.; Nampaawu, M.J.; Kakaire, D.; et al. The epidemiology and outcomes of adults with acute hypoxaemic respiratory failure in a low-income country in the context of the COVID-19 pandemic. BMJ Glob. Health 2025, 10, e017949. https://doi.org/10.1136/bmjgh-2024-017949
43. [43] Mikami, Y.; Grubb, B.R.; Rogers, T.D.; Dang, H.; Asakura, T.; Kota, P.; Gilmore, R.C.; Okuda, K.; Morton, L.C.; Sun, L.; et al. Chronic airway epithelial hypoxia exacerbates injury in muco-obstructive lung disease through mucus hyperconcentration. Sci. Transl. Med. 2023, 15, eabo7728. https://doi.org/10.1126/scitranslmed.abo7728
44. [44] Derscheid, R.J.; van Geelen, A.; Berkebile, A.R.; Gallup, J.M.; Hostetter, S.J.; Banfi, B.; McCray, P.B. Jr.; Ackermann, M.R. Increased concentration of iodide in airway secretions is associated with reduced respiratory syncytial virus disease severity. Am. J. Respir. Cell Mol. Biol. 2014, 50, 389–397. https://doi.org/10.1165/rcmb.2012-0529OC
45. [45] Bastani, M.N.; Jalilian, S. Unraveling the enigma: the emerging significance of pulmonary surfactant proteins in predicting, diagnosing, and managing COVID-19. Immun. Inflamm. Dis. 2024, 12, e1302. https://doi.org/10.1002/iid3.1302
46. [46] Fontela, P.C.; Berwanger, O.; Cavalcanti, A.B.; Tanaka, L.M.S.; Daltro-Oliveira, R.; Lobo, S.M.; Lacerda, M.V.G.; Moura, A.D.T. New and personalized ventilatory strategies in patients with COVID-19. Front. Med. 2023, 10, 1194773. https://doi.org/10.3389/fmed.2023.1194773
47. [47] Abou-Ismail, M.Y.; Diamond, A.; Kapoor, S.; Arafah, Y.; Nayak, L. The hypercoagulable state in COVID-19: incidence, pathophysiology, and management. Thromb. Res. 2020, 194, 101–115. https://doi.org/10.1016/j.thromres.2020.06.029
48. [48] Genzel, L.; Akgul, G.; Abel, T.; Bhatt, D.L.; Bhatt, S.; Birmingham, K.; Bishnoi, I.R.; Bhatt, M.; Bhatt, V.; et al. Animal models for the study of SARS-CoV-2-induced respiratory disease and pathology. Comp. Med. 2023, 73, 85–103. https://doi.org/10.30802/AALAS-CM-22-000049
49. [49] Zhong, M.; Gao, Y.; Hu, H.; Zhu, X.; Gan, L.; Li, L.; Xiang, C.; Yan, Y.; Dai, Z. Transient low T3 syndrome in patients with COVID-19: a new window for prediction of disease severity. Front. Endocrinol. 2023, 14, 1154007. https://doi.org/10.3389/fendo.2023.1154007
50. [50] Colella, C.; Baldelli, R.; Saba, L.; Granata, A. Non-thyroidal illness syndrome and thyroid autoimmunity in hospitalized COVID-19 patients: a retrospective study. J. Clin. Med. 2025, 14, 6784. https://doi.org/10.3390/jcm14196784
51. [51] Deng, J.; Zhang, S.; Peng, F.; Zhang, Q.; Li, Y.; Zhong, Y. The association between fT3 with the outcome and inflammation/coagulopathy/fibrinolysis of COVID-19. Front. Endocrinol. 2022, 13, 877010. https://doi.org/10.3389/fendo.2022.877010
52. [52] Rada, B.; Gardina, P.; Myers, T.G.; Trinchieri, G. Antimicrobial actions of dual oxidases and lactoperoxidase. J. Microbiol. 2018, 56, 373–386. https://doi.org/10.1007/s12275-018-7545-1

Disclaimer/Publisher's Note: The statements, opinions and data contained in all publications are solely those of the individual author(s) and contributor(s) and not of MDPI and/or the editor(s). MDPI and/or the editor(s) disclaim responsibility for any injury to people or property resulting from any ideas, methods, instructions or products referred to in the content.

© 2026 by the author(s). Distributed under a Creative Commons CC BY license.